journal

J. Am. Ceram. Soc., 88 [9] 2362–2368 (2005)
DOI: 10.1111/j.1551-2916.2005.00449.x

Enhanced Sintering of Yttrium-Doped Barium Zirconate by Addition of ZnO

Peter Babilo and Sossina M. Haile†

Department of Materials Science, California Institute of Technology, Pasadena, California 91125

The influence of transition metal oxides additives, especially zinc oxide, on the densification and electrical properties of doped barium zirconate have been examined. With the use of zinc oxide as a sintering aid, $BaZr_{0.85}Y_{0.15}O_{3-\delta}$ was readily sintered to above 93% of theoretical density at 1300°C. Scanning electron microscopic investigations showed Zn accumulation in the intergranular regions. Thermogravimetric analysis of the material under flowing CO_2 showed ZnO-modified barium zirconate to exhibit excellent chemical stability. The conductivity, as measured by A.C. impedance spectroscopy under H_2O saturated nitrogen, was slightly lower than that of unmodified barium zirconate. Electromotive force measurements under fuel cell conditions revealed the total ionic transport number to be ~0.9 at 600°C. The combination of electrical and chemical properties and good sinterability render ZnO-modified barium zirconate an excellent candidate for reduced temperature solid oxide fuel cell applications.

I. Introduction

Many alkaline earth perovskites exhibit high proton conductivities at moderately elevated temperatures (400°–700°C). These materials have attracted attention for their potential applications as electrolytes in fuel cells and chemical sensors.[1–5] Examples with well-documented proton conductivities include barium cerate ($BaCeO_3$),[2,6–8] strontium cerate[9] and the perovskite-derivative BCN.[10–12] Many of these compounds suffer from chemical instability under CO_2 containing atmospheres, readily forming alkaline earth carbonates according to Eq. (1)[13,14]

$$BaCeO_3 + CO_2 \rightarrow BaCO_3 + CeO_2 \quad (1)$$

This reactivity causes severe degradation of the electrolyte and precludes applications in fuel cells based on hydrocarbon fuels.

In contrast, barium zirconate exhibits excellent stability under CO_2,[15,16] rendering it highly attractive for applications in aggressive environments. While initial investigations suggested that barium zirconate did not share the high proton conductivity of other members of the alkaline earth perovskite family,[15,17] it has been more recently recognized that doped $BaZrO_3$, in fact, exhibits higher bulk conductivity than doped $BaCeO_3$.[18–20] The early mis-interpretation of the behavior of doped barium zirconate originates from the highly refractory nature of this material, which results in samples with small grain sizes and high total grain-boundary area. As a consequence, the resistive grain boundaries produce a material with an overall low conductivity, and, in the absence of low temperature A.C. impedance measurements (< ~200°C), the individual bulk and grain-boundary contributions to conductivity were not resolved in the early literature.

The refractory nature of doped barium zirconate leads to significant challenges to its implementation in fuel cells and other devices. First, it is difficult to process to a high density (>93%), as is required of fuel cell electrolyte membranes. Typically, extreme conditions, such as high temperature (1700°–1800°C), long sintering times (24 h), and nanometer-sized particles are needed to prepare fully densified pellets.[13,19,21,22] Not only are these conditions costly to implement, they are incompatible with most potential electrode materials and thereby preclude the fabrication of co-sintered structures. Second, it is the total resistance of the electrolyte, not only that of the bulk or grain interiors, that dictates electrochemical performance. Thus, strategies for improving total grain-boundary conductivity are required. Third, high temperature processing can be anticipated to induce barium oxide evaporation and thereby decrease conductivity, as has been observed in $BaCeO_3$.[13] In addition, occasional abnormal grain growth[19] results in inhomogeneous properties, both electrical and mechanical, which are highly undesirable.

In the present work, we demonstrate that ZnO is an effective sintering aid for $BaZr_{0.85}Y_{0.15}O_{3-\delta}$ (BYZ), enhancing both densification and uniform grain growth. Yttrium has been selected as the dopant because of the high proton conductivity this species imparts, presumably as a result of its good ionic radius match to Zr.[15] Of potential sintering aids, a previous study of Al_2O_3, MgO, and Y_2O_3 on barium zirconate densification showed a marginal improvement in sintering behavior with yttria. This additive yielded samples of 91%–92% dense at 1600°C as compared with ~90% density for pristine samples processed under identical conditions.[23] While no detailed mechanism for the slight enhancement in density was presented, it was speculated that yttria limits grain growth.‡ In this work, an initial screening of all transition elements in the series Sc to Zn, as discussed below, showed NiO, CuO, and ZnO to be the most effective additives for enhancing barium zirconate densification. Of these, zinc oxide was selected as most suitable and accordingly subjected to further investigation and system optimization.

II. Experimental Procedure

(1) Sample Preparation

Crystalline powders of BYZ were synthesized by a glycine-nitrate combustion synthesis process.[24] Starting materials were high purity $Ba(NO_3)_2$ (Alfa Aesar, 99.95% purity), $Y(NO_3)_3 \cdot 6H_2O$ (Alfa Aesar, 99.9% purity), and $ZrO(NO_3)_2 \cdot xH_2O$ (Alfa Aesar, Ward Hill, MA, 99.9% purity), where $x = 2.3$, as determined by thermogravimetric analysis (TGA). The appropriate molar ratios of nitrates and glycine (NH_2CH_2COOH) were mixed in a minimum volume of deionized water to obtain a transparent solution. A glycine to nitrate ratio of 1:3 was used. The aqueous solution was dehydrated on a hot plate at a temperature of 150°C

J. Drennan—contributing editor

Manuscript No. 20302. Received July 26, 2004; approved March 14, 2005.
Funding for this work was provided by the Department of Energy, Office of Energy Efficiency and Renewable Energy, and by the Army Research Office, Chemical Science Division, through subcontract with NexTech, Inc. Additional support has been provided by the National Science Foundation, through the Caltech Center for the Science and Engineering of Materials.
†Author to whom correspondence should be addressed. e-mail: smhaile@caltech.edu

‡Although it was suggested that yttria additive limits grain growth in barium zirconate, from an examination of the micrographs presented, this does not appear to be the case.

generating a viscous liquid. Upon complete evaporation of the water, the viscous liquid autoignited to produce the desired powders. After autoignition, powders were calcined at 1000°C for 2 h to yield well-crystallized BYZ powders, which were subsequently attritor milled at 550 rpm for 2 h to produce uniform, submicrometer particles with approximate surface area of 8 m^2/g.

Preliminary modifier screening experiments were carried out by mechanical addition of 4 mol% of the transition metal oxide (Alfa Aesar, 99.9%–99.99% purity) to the BYZ powder synthesized as described above. The stoichiometry of the BYZ base material was not adjusted to accommodate the modifier and no assumption about site incorporation mechanisms were made. In the case of ZnO, two additional synthesis routes were explored. The first involved dissolution of zinc nitrate (Alfa Aesar, 99% purity) directly into the BYZ nitrate solution described above, with stoichiometry adjusted to reflect incorporation of the Zn in the B site of the perovskite ($BaY_{0.15}Zn_{0.04}Zr_{0.81}O_3$). In the second method, ZnO (Alfa Aesar, 99.99% purity, surface area of 8.5 m^2/g) was introduced as an oxide powder to the BYZ nitrate solution just prior to complete dehydration. With the latter technique, the stoichiometry of the BYZ base materials was not adjusted to accommodate the ZnO.

$BaCeO_3$, for comparison of chemical stability with BYZ, was synthesized via the glycine-nitrate combustion synthesis in a process similar to the one described above. The cerium source was $Ce(NO_3)_3 \cdot 6H_2O$ (Alfa Aesar, 99.9% purity).

(2) Sample Characterization

The X-ray diffraction (XRD) analyses of calcined powder samples were performed at room temperature using a Phillips diffractometer (X'Pert Pro) with Cu$K\alpha$ radiation. Intensities were obtained in the 2θ range between 20° and 80° with a step size of 0.02° and a measuring time of 3 s at each step.

Densification studies were performed both by direct measurements of sample density and linear shrinkage after sintering at a specified temperature and by dilatometry. Green pellets (10 mm in diameter, 1–2 mm thickness) were obtained by pressing ceramic powders uniaxially at 400 MPa for 30 s. Sintering was carried out at temperatures between 1300° and 1700°C (4 h) under a stagnant air atmosphere. Densities of sintered samples were determined using the Archimedes method using water as the immersion medium. Total linear shrinkage ($(l - l_0)/l_0$, where l_0 is the initial length and l is the final length) resulting from sintering was established from direct measurements of sample dimensions before and after sintering. Dilatometry experiments, permitting *in situ* measurements of linear shrinkage as a function of temperature, were performed with a dilatronic dilatometer (Theta Industries Inc., Port Washington, NY). Data were collected at a heating rate of 3°C/min under a stagnant air atmosphere.

The microstructure and chemical composition of sintered samples were investigated by means of scanning electron microscopy (LEO 1550VP Field Emission SEM, Zeiss, Oberkochen, Germany) in conjunction with energy dispersive X-ray spectroscopy (EDS, Oxford INCA Energy 300, Fremont, CA). The exposed top surface of the sample was polished in preparation for chemical analysis. The Oxford INCA EDS software employs the Pouchou and Pichoir (PAP) model for quantitative analysis[25] in which fundamental factors are used to correct for the effects of atomic number, absorption, and fluorescence to the measured intensity of the elements. Accordingly, standards are not necessary.

In order to assess chemical stability, TGA of selected samples was carried out under flowing CO_2 ($P_{CO_2} = 0.20$) using a Netzsch 499 STA (Exton, PA). For this purpose, samples were lightly sintered to a density of 60%–65% of theoretical.

The conductivity of densified pellets of 4 mol% ZnO-modified BYZ (BYZ-Zn4) were measured under water-saturated nitrogen in the temperature range of 50°–350°C. The BYZ-Zn4 sample was that prepared by the zinc oxide+BYZ nitrate route and sintered at 1300°C for 4 h (93% dense). A.C. impedance data were collected over the frequency range of 10^3–10^6 Hz using a HP 4284A precision LCR meter (Agilent, Palo Alto, CA) at an applied voltage of 1 V. It should be noted that the samples were not electrochemically decomposed because of the voltage bias. Platinum electrodes were sputtered onto the surfaces of polished samples. The least squares refinement program ZView (Scribner Associates Inc., Southern Pines, NC) was employed to fit the acquired impedance data to an $(R_1Q_1)(R_2Q_2)$ equivalent circuit, where R is resistance and Q is constant phase element with impedance $Z_Q = (Y(j\omega)^n)^{-1}$;[26] where $j = \sqrt{-1}$, ω = frequency, Y and n are constants, and n ranges between 0 and 1.

The ionic transport number of the same material was obtained from electromotive force (EMF) measurements. A pellet with dimensions 17 mm in diameter and 1–2 mm in thickness was prepared with porous Pt electrodes (Engelhard 6082, Iselin, NJ) pasted onto both sides of the disc. The sample was affixed to the end of a quartz tube with a gas-tight ceramic paste seal (Aremco Ceramabond 552, Valley Cottage, NY). A voltage was generated by exposing the two electrode surfaces to different atmospheres. Specifically, one surface was exposed to water-saturated hydrogen and the other to water-saturated compressed air ($P_{H_2O} = 0.03$ bar):

$$H_2, H_2O, Pt|sample|Pt, H_2O, O_2$$

The governing chemical reaction in this case is simply hydrogen and oxygen combining to form water:

$$H_2 + \tfrac{1}{2}O_2 \rightarrow H_2O \tag{2}$$

The theoretical or Nernstian voltage, E_N, expected from this reaction is

$$E_N = E_0 + \frac{RT}{2F} \ln\left(\frac{P_{O_2}^{0.5} P_{H_2}}{P_{H_2O}}\right) \tag{3}$$

where $E_0 = \Delta G_0 / 2F$, ΔG_0 is the Gibbs free energy of the reaction under standard conditions ($T = 273$ K, $P = 1$ bar),[27] R is the universal gas constant, T is temperature, F is Faraday's constant and P_{H_2}, P_{O_2}, P_{H_2O} are the partial pressures of hydrogen, oxygen, and water, respectively. The ionic transport number was calculated from the ratio of the measured EMF to this Nernstian value, $t_{ion} = E_{meas}/E_N$.

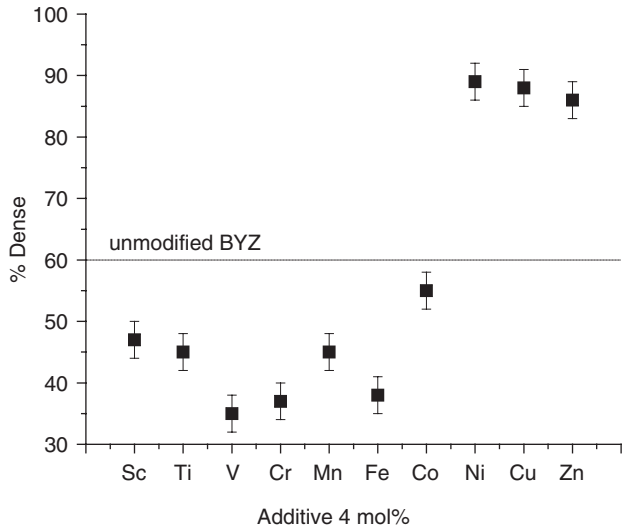

Fig. 1. Effect of transitional metal oxide additives as sintering aids for $BaZr_{0.85}Y_{0.15}O_{3-\delta}$ (BYZ).

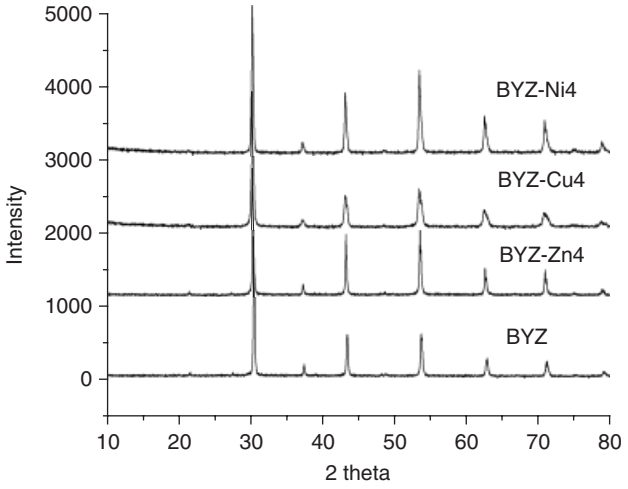

Fig. 2. X-ray powder diffraction patterns of sintered $BaZr_{0.85}Y_{0.15}O_{3-\delta}$ (BYZ), BYZ-Zn4, BYZ-Cu4, and BYZ-Ni4.

III. Results and Discussion

(1) Preliminary Comparison of Transition Metal Modifiers

Densities obtained from 4 mol% transition-metal modified BYZ samples, sintered at 1300°C with a 4 h soak time, are shown in Fig. 1. As evident from the data, Ni, Cu, and Zn are tremendously effective in enhancing densification, raising the final density from about 60% of theoretical for the unmodified material to approximately 86%–88% for modified BYZ. Other additives such as V, Cr, and Fe, in contrast, substantially worsened densification behavior. Diffraction patterns obtained after sintering, from BYZ modified with the favorable elements, are presented in Fig. 2. In all cases, a single perovskite phase is indicated. However, upon closer examination under the SEM (not shown here) the Cu modified sample showed the presence of $Ba_2YCu_3O_x$. In addition, both this material and the Ni-modified BYZ pellet changed color from white to black upon sintering. In contrast, the Zn-modified sample acquired a pale green color. Often, black coloring in an oxide indicates substantial electronic conductivity, and even though the transition metal concentration in these samples is low, suggesting the electronic transference number would not be large, Cu and Ni were abandoned as modifiers in favor of Zn.

The impact of ZnO content on the sintering behavior of BYZ (samples prepared by mechanical mixing of the two oxides, 1300°C, 4 h) is presented in Fig. 3. Densification, as measured in terms of total linear shrinkage, dramatically increased in the range from 0 to 4 mol% Zn, then remained at a constant intermediate value for higher Zn concentrations. Although this behavior was established only for Zn in particular, it is because of this concentration dependence of densification that 4 mol% was selected for the preliminary screening of transition metal elements as modifiers. The impact of different methods of ZnO addition on the densification of BYZ is also presented in Fig. 3, in which the linear shrinkage of BYZ-Zn4 prepared by the three different routes are compared. Of the three BYZ-Zn4 samples, densification is greatest for ZnO introduced as a dispersed oxide into the BYZ nitrate solution. The improvement over mechanical mixing of the two oxides is attributed to the greater homogeneity of the ZnO distribution within the ceramic sample. The poorer densification of the presumably most homogenous sample, that in which zinc nitrate was added to the BYZ nitrate solution, is attributed to the complete dissolution of Zn into the bulk crystalline structure of BYZ without significant preferential segregation to the grain boundaries. In comparison with the unmodified sample, however, even this sample shows enhanced shrinkage over simple BYZ. All subsequent studies were performed with materials prepared via introduction of zinc oxide to the BYZ nitrate solution.

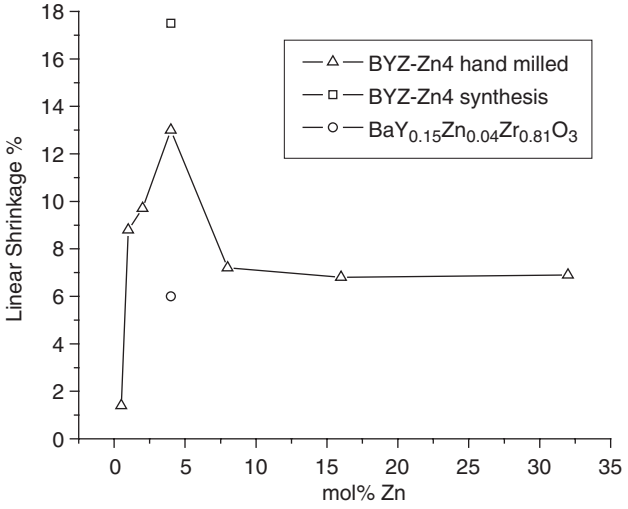

Fig. 3. Linear shrinkage of Zn modified $Ba(Zr_{0.85}Y_{0.15})O_3$ after sintering at 1300°C in air (4 h) as a function of mole percentage of ZnO. △, mechanical addition; □, Zn oxide addition to BYZ nitrate solution; ○, zinc nitrate addition to BYZ nitrate solution.

(2) Densification with ZnO

The difference in sintering behavior between unmodified and Zn-modified BYZ is particularly evident from a comparison of the dilatometry curves obtained from the two materials, Fig. 4. The onset of sintering in BYZ-Zn4, occurs at approximately 1000°C, 200°C before its onset in the BYZ system. Furthermore, between 1000° and 1100°C, BYZ-Zn4 shrinkage is ~4%, whereas it is only ~1% for BYZ over the analogous temperature range of 1200°–1300°C. At 1300°C, the total linear shrinkage for BYZ-Zn4 is 17.5% (as compared with only ~1% for BYZ).

Additional comparisons between the behavior of BYZ-Zn4 (optimally synthesized) and unmodified BYZ are presented in Figs. 5 and 6, in which the post-sintering densities as a function of temperature and selected micrographs, respectively, are shown. As evident from Fig. 5, the maximum densities that could be achieved from these two materials differ significantly: 95% of theoretical for BYZ-Zn4 ($\rho_{theo} = 6.12$ g/cm^3), at a sintering temperature of 1300°C, compared with only 88% for BYZ, at a sintering temperature 1700°C. At 1300°C, the density of unmodified BYZ is only ~60%. The electron micrograph images for the two different samples obtained after sintering at 1300°C confirm the macroscopic observations. The BYZ system has considerable porosity (~40%) after sintering at this low

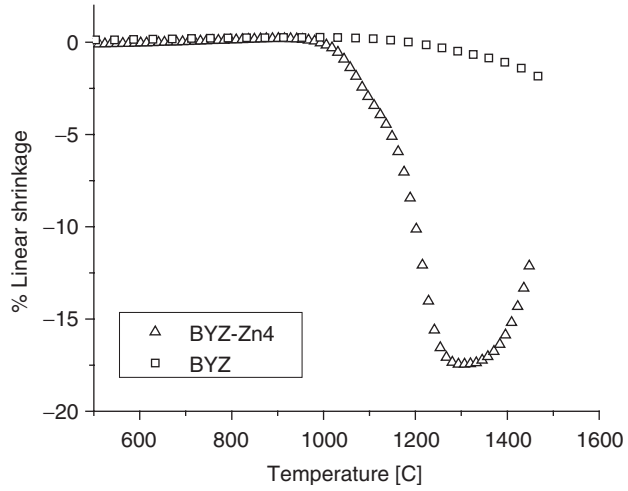

Fig. 4. Temperature dependence of linear shrinkage in $BaZr_{0.85}Y_{0.15}O_{3-\delta}$ (BYZ) and BYZ-Zn4.

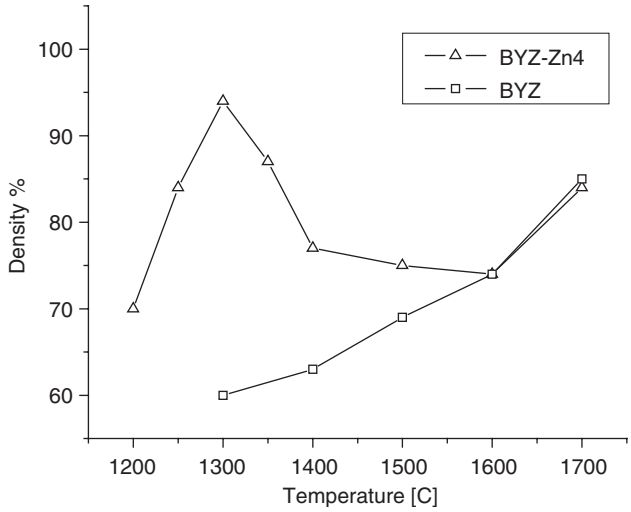

Fig. 5. Density of $BaZr_{0.85}Y_{0.15}O_{3-\delta}$ (BYZ) and BYZ-Zn4 as a function of sintering temperature in ambient atmosphere.

temperature, Fig. 6(a), whereas the BYZ-Zn4 system appears dense and exhibits a larger average grain size, Fig. 6(b) (0.30 vs 1.0 μm). The images (examined in combination with EDS chemical analysis) furthermore reveal that the BYZ-Zn4 system is free of secondary phases.

The temperature dependence of sample density differs dramatically between the Zn-modified and unmodified materials, Fig. 5. For the former a highly obvious maximum in density as a function of sintering temperature exists, occurring at 1300°C, whereas the latter shows a monotonically increasing density as a function of sintering temperature. The dilatometry data, Fig. 4, similarly shows a loss in density for BYZ-Zn4 exposed to temperatures above 1300°C. This decrease in density is accompanied by an unusual change in microstructure, Fig. 6(c), in which individual grains can no longer be distinguished. The decreasing density of BYZ-Zn4 is thought to result from evaporation of Zn at elevated temperatures according to

$$ZnO(s) \longleftrightarrow Zn(g) + \tfrac{1}{2}O_2(g) \quad (4)$$

This conclusion is supported by preliminary observations that ZnO is effective as a sintering additive only in relatively oxidizing atmospheres (air). Under reducing atmospheres, Eq. (4) is driven to the right and metallic zinc readily vaporizes. Indeed, under an atmosphere with 10^{-6} bar O_2 partial pressure, the partial pressure of Zn at 1300°C, based on available thermodynamic data,[28] is approximated as 10^{-2} bar, indicating significant zinc loss.

(3) Chemical Analysis

The diffraction and microscopy studies, Figs. 1 and 6, respectively, indicate that BYZ-Zn4 is free of obvious secondary phases, which may have served to enhance sintering through the formation of a eutectic melt. However, these techniques provide little information about the distribution of Zn within the polycrystalline perovskite. Of particular relevance is whether there is any difference in Zn concentration between bulk and grain-boundary regions. The results of chemical analysis as determined by quantitative analysis of the EDS spectra are presented in Table I (for BYZ-Zn4 sintered at 1300°C). The mole percentages are normalized to one unit of barium. The bulk composition appears slightly barium deficient, possibly an artifact of the experimental technique in that EDS rather than more quantitative wavelength dispersive X-ray spectroscopy (WDS) has been employed. More importantly, within the detection limit, there is no Zn within the grain interiors. In contrast, the grain boundaries have a substantial concentration of Zn, almost 5 mol%, and this coincides with a decrease in the Y concentration by about 3 mol% relative to that in the bulk. Furthermore, the grain boundaries exhibit a slightly greater barium deficiency.

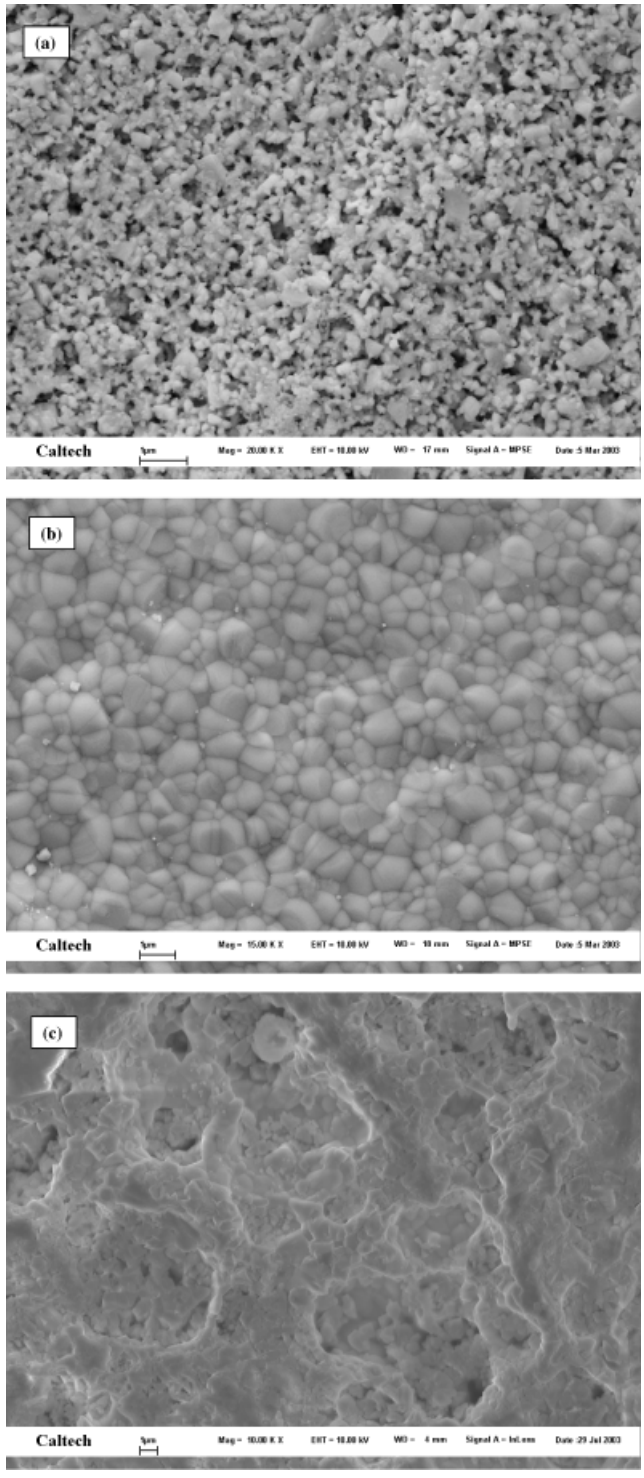

Fig. 6. SEM surface micrograph of sintered (a) $BaZr_{0.85}Y_{0.15}O_{3-\delta}$ (BYZ) at 1300°C, (b) BYZ-Zn4 at 1300°C, and (c) BYZ-Zn4 at 1400°C.

In light of the chemical analysis, the enhanced densification observed here is assumed to be a result of the high Zn concentration in the grain-boundary regions. Given the larger mean grain size of BYZ-Zn4 than simple BYZ for samples sintered at 1300°C, Fig. 6, it is apparent that Zn increases rather than decreases grain-boundary mobility. In stark contrast, Caballero *et al.*[29] observed that introduction of very small concentrations of ZnO to $BaTiO_3$ dramatically inhibited grain growth but, nevertheless, marginally improved densification. Grain-boundary mobility in oxides is limited by the diffusivity of the slowest

Table I. Chemical Compositional Comparison of the Bulk and Grain Boundary in the BYZ-Zn4 Densified System

	Zn	Y	Zr	Ba	O
Bulk	0.000	0.099	0.914	1.000	2.947
Bulk	0.000	0.126	0.936	1.000	3.025
Bulk	0.003	0.166	0.928	1.000	3.107
Bulk	0.000	0.099	0.915	1.000	2.972
Average bulk	0.001	0.123	0.923	1.000	3.013
Grain	0.012	0.085	0.915	1.000	2.970
Grain	0.057	0.091	0.930	1.000	3.053
Grain	0.078	0.087	0.936	1.000	3.080
Grain	0.047	0.104	0.951	1.000	3.104
Average grain	0.049	0.092	0.933	1.000	3.052

BYZ, $BaZr_{0.85}Y_{0.15}O_{3-\delta}$.

moving species[30] and in the case of perovskites these are the cations. In the grain-boundary regions of BYZ-Zn4, the Zn appears to be incorporated on the B site of the perovskite, which could be expected to increase the vacancy concentrations on both the Ba and oxygen sites:

$$ZnO \rightarrow Zn''_{Zr} + O_O + V''_{Ba} + 2V^{\bullet\bullet}_O \quad (5)$$

The increase in barium vacancy concentration, may, in turn, be responsible for the increase in grain-boundary mobility, grain growth, and densification. Such a mechanism may also, in part, explain the marginal impact of Zn on BYZ sintering when added to yield an overall composition of $Ba(Zr_{1-x}Y_yZn_z)O_{3-\delta}$, as was the case for the samples in which zinc nitrate was directly introduced into the BYZ nitrate solution.

(4) Chemical Stability

A comparison of the thermal gravimetric behavior of BYZ, BYZ-Zn4 and $BaCeO_3$ in the presence of CO_2 is presented in Fig. 7. Consistent with earlier observations,[13] gradual weight gain is apparent for the $BaCeO_3$ above 600°C signifying the formation of $BaCO_3$ as per Eq. (1). In contrast, BYZ and BYZ-Zn4 show no significant weight gain. Thus, the ZnO additive does not impact the excellent stability of barium zirconate in carbon dioxide containing atmospheres.

(5) Transport Properties

Nyquist plots (Z_{real} versus Z_{imag} as parametric functions of frequency) obtained at selected temperatures for BYZ-Zn4 under water-saturated nitrogen are shown in Fig. 8. In the temperature range of 120°–160°C, the impedance spectra consisted of two

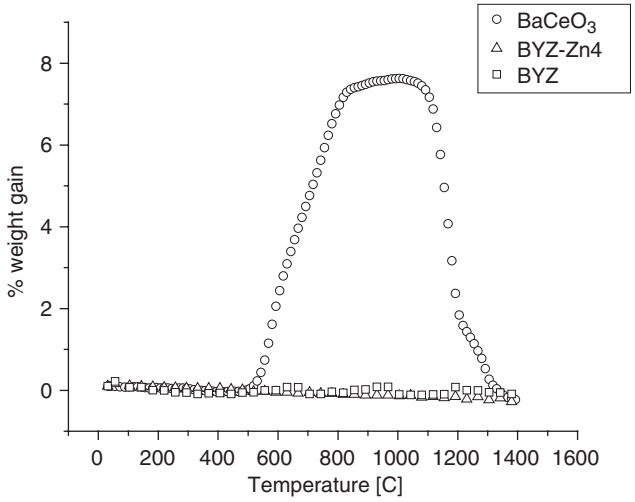

Fig 7. Thermogravimetric analysis of $BaZr_{0.85}Y_{0.15}O_{3-\delta}$ (BYZ)-Zn4 and BYZ as compared with $BaCeO_3$ in a CO_2 atmosphere.

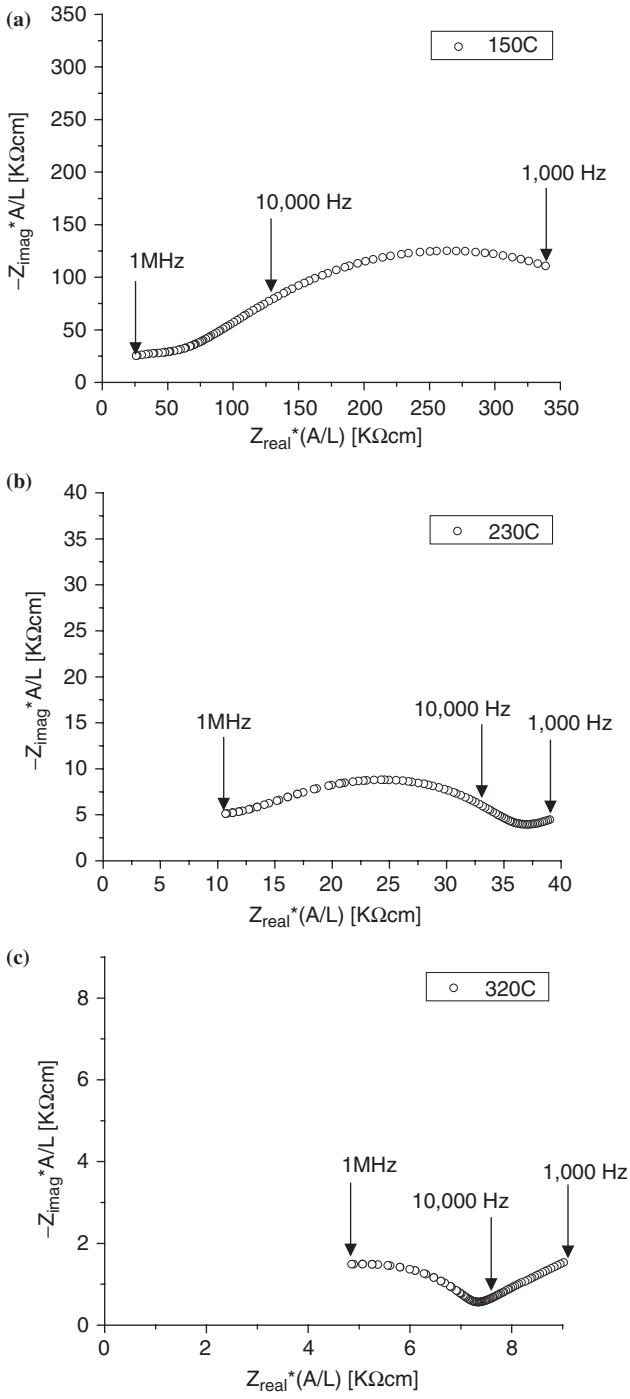

Fig. 8. Nyquist impedance plots for $BaZr_{0.85}Y_{0.15}O_{3-\delta}$ (BYZ)-Zn4 obtained at (a) 150°C, (b) 230°C, and (c) 320°C in water-saturated nitrogen atmosphere.

semicircles. The low frequency arc is attributed to grain-boundary processes whereas the high frequency arc is attributed to the bulk response.[17,18,31] With increasing temperature, these two arcs shift towards higher frequencies and by ~230°C a third feature, which corresponds to the electrode response, appears at the low frequency end of the spectrum.[17,20,32] At a temperature of ~250°C the characteristic frequency of the bulk response reaches a value greater than the maximum measurement frequency of the impedance meter and thus the bulk arc is no longer accessible.

After least squares fitting to the impedance data to obtain the resistances associated with the high and intermediate frequency arcs, the conductivities of the bulk and grain-boundary regions were deduced by accounting for the sample geometry according

to Eq. (6):

$$\sigma = \frac{1}{R}\frac{L}{A} \tag{6}$$

where L is the sample thickness and A is its cross-sectional area. The grain-boundary conductivity obtained from this simple calculation is a measure of both the grain-boundary geometry (i.e. sample microstructure) and the inherent properties of the grain boundaries. The specific grain-boundary conductivity (independent of microstructure), $\sigma_{sp.gb}$, was determined using the approximation:[31]

$$\sigma_{sp.gb} = \frac{L}{A}\left(\frac{C_{bulk}}{C_{gb}}\right)\frac{1}{R_{gb}} \tag{7}$$

where C is capacitance, given by $C = Y^{(1/n)}R^{(\frac{1}{n}-1)}$, R is resistance, and Y and n are the parameters associated with the constant phase element. A temperature averaged (single) value of the ratio C_{bulk}/C_{gb} ($=0.0182$) was employed for these calculations.

The temperature dependences of the bulk (or grain interior), total grain boundary and specific grain-boundary conductivities of BYZ-Zn4 (with a mean grain size of ~ 1 μm) are presented in Fig. 9. The data obtained from BYZ-Zn4 are compared with the bulk conductivity of $BaZr_{0.90}Y_{0.10}O_3$ (BYZ10) as reported by Bohn and Schober,[20] and to the specific grain-boundary conductivity of $BaCe_{0.85}Gd_{0.15}O_3$ as reported by Haile *et al.*[31] In Table II are listed the activation energies, E_a, and pre-exponential terms, A, determined from a fit of the data to the Arrhenius equation

$$\sigma T = A\,\exp(-E_a/k_b T) \tag{8}$$

where T and k_b are temperature and the Boltzman constant, respectively.

From the results presented in Fig. 9, it is immediately apparent that the bulk conductivity of BYZ-Zn4 is lower than that of BYZ10, by a factor of two. Furthermore, differences appear in both the activation energy for proton transport, 0.47 vs 0.44 eV for BYZ-Zn4 and BYZ10, respectively, and the pre-exponential term, $10^{3.51}$ vs $10^{3.65}$, respectively. This result is surprising in light of the chemical analysis, which suggests that little if any Zn is incorporated within the bulk structure of BYZ-Zn4. Moreover, the dopant (yttrium) concentration in BYZ-Zn4, 15%, is greater than in BYZ10, 10%, suggesting a higher proton concentration and thus larger pre-exponential term in the material studied here. That the opposite is observed indicates that even at the lowest levels, Zn has a detrimental impact on bulk conductivity. We speculate that Zn^{2+} ions residing on the tetravalent Zr site, with effective -2 charge, act as deep proton traps, both decreasing the effective concentration of protons able to participate in the charge transport process and raising the activation energy. We note that preliminary measurements of high density (unmodified) BYZ[33] yield bulk conductivity values that are almost identical to those of Bohn and Schober, and thus the differences between BYZ10 and BYZ-Zn4 are not due to experimental artifacts.

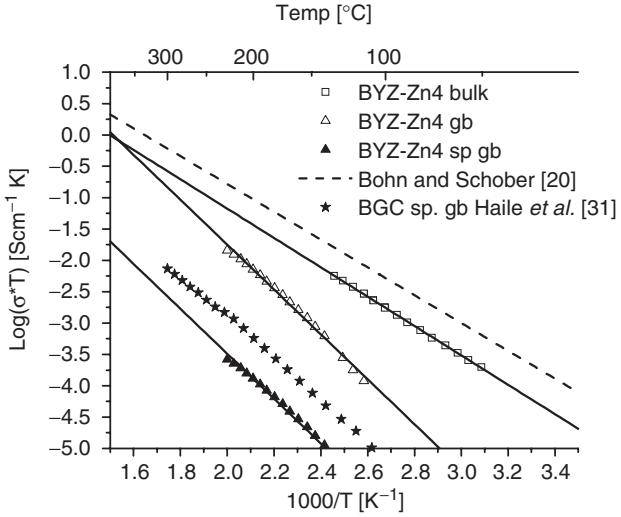

Fig. 9. The bulk, total grain boundary, and specific grain-boundary conductivity of $BaZr_{0.85}Y_{0.15}O_{3-\delta}$ (BYZ)-Zn4 as a function of temperature plotted in Arrhenius form. Atmosphere is water-saturated nitrogen. Data are compared with those of Bohn and Schober[20] for the bulk conductivity of unmodified $BaZr_{0.9}Y_{0.1}O_3$ and those of Haile *et al.*[31] for the specific grain-boundary conductivity of $BaCe_{0.85}Gd_{0.15}O_3$.

Table II. Comparison of Activation Energies and Pre-Exponential Factor of Bulk and Grain-Boundary Conductivity of BYZ-Zn4 and BYZ

	BYZ-Zn4	Bohn and Schober[20]
E_a, bulk (eV)	0.47 (1)	0.44
Log A, bulk (K S/cm)	3.51	
E_a, gb (eV)	0.71 (1)	0.7
Log A, sp.gb (K S/cm)	3.67	
Log A, tot.gb (K S/cm)	5.41	

BYZ, $BaZr_{0.85}Y_{0.15}O_{3-\delta}$; sp.gb, specific grain-boundary; tot.gb, total grain-boundary.

A comparison of the grain-boundary properties of BYZ10 and BYZ-Zn4 reveals another surprising result. In this case (Bohn and Schober data not shown), there is very little difference between the two samples, despite the very high concentration of Zn in the grain-boundary regions of BYZ-Zn4. The activation energies are comparable (~ 0.7 eV) and the pre-exponential terms for the total grain-boundary conductivities, which include effects of both the specific grain-boundary properties and the microstructure, are $\sim 10^{5.3}$ (BYZ-Zn4 total conductivity data not shown). It is possible that even in nominally pure BYZ10, impurities accumulate in the grain-boundary region and dominate the proton transport process, giving rise to grain boundary properties that are similar to those of BYZ-Zn4. Both BYZ-Zn4 and BYZ10 are similar to gadolinium doped $BaCeO_3$,[31] in that the activation energy for grain-boundary transport is higher than through the bulk, and, furthermore that the specific grain-boundary conductivity is several orders of magnitude lower than that of the bulk. Although the specific grain-boundary conductivity of BYZ10 was not reported (nor was the grain size), it is possible to deduce this conclusion from the simple observation of a grain-boundary arc.[31] In terms of the cerate, the observation of high grain-boundary resistance has been explained in terms of the disruption of the perovskite structure, which is otherwise favorable to rapid proton transport, at disordered grain-boundary regions. Perhaps more significantly, Fig. 9 reveals that of the specific grain-boundary conductivity of BYZ-Zn4 is lower than that of $BaCeO_3$. Thus, not only does the high concentration of grain boundaries in barium zirconate decrease total conductivity relative to the cerate, so do the inherent properties of those boundaries. Therefore, optimization of transport properties relies heavily on the ability to grow grains to moderate sizes so as to reduce total grain-boundary area. Modification of BYZ with ZnO enhances grain growth and addresses precisely this challenge, although further optimization will be necessary in order to obtain total grain-boundary conductivity that is greater than that of unmodified BYZ.

The results of the EMF measurements are summarized in Table III. The data reveal the ion transport number of BYZ-Zn4 to be ~ 0.90 in the temperature range of interest, dropping slightly from 0.90°C at 500°C to 0.86°C at 700°C. By analogy to related materials[2] the balance of the charge transport can be attributed to electron hole charge carriers. With increasing tem-

Table III. Ionic Transport Number of BYZ-Zn4 as a Function of Temperature

		T (°C)	Measured EMF (mV)	Theoretical EMF (mV)	t_{ion}
BYZ-Zn4					
Cathode	Anode				
Air-3%H_2O	H_2-3%H_2O	700	966	1120	0.86
		650	990	1128	0.88
		600	1017	1136	0.90
		550	1030	1144	0.90
		500	1037	1152	0.90

BYZ, $BaZr_{0.85}Y_{0.15}O_{3-\delta}$.

perature, both the loss of water from the structure and the higher mobility of the holes lead to a slight decrease in ionic transport number. The value shown here is somewhat higher than reported by Schober and Bohn[19] for unmodified BYZ10, who obtained ~0.8 at 700°C for a similar but not identical EMF cell. The higher EMF values in the present work are more likely because of the more reducing conditions employed at the anode or slightly higher dopant concentration rather than to an inherent improvement in ionic transference number upon introduction of Zn. Overall, it is apparent that the ionic transport number of BYZ-Zn4 is large enough for satisfactory implementation in a fuel cell.[34]

(6) Summary

A homogeneous distribution of ZnO in the intergranular regions of BYZ leads to enhanced, yet relatively uniform, grain growth of the host oxide, which, in turn, results in high densities (>93%) at reduced sintering temperatures (1300°C). Chemical analysis by EDS methods confirms the accumulation of Zn at the grain boundaries. In the absence of a second phase, sintering is believed to take place by enhanced solid-state diffusion, possibly because of cation vacancy formation in the intergranular regions. Despite the apparent absence of Zn from the grain interiors, the bulk conductivity of zinc oxide modified BYZ is lower than that of unmodified BYZ. At the same time, the total grain-boundary conductivity appears largely unaffected by the ZnO modifier, despite the high concentration of Zn at the grain boundaries and presumably larger grain size. The reduction in bulk conductivity may be because of strong proton trapping at Zn''_{Zr} sites, which are present in levels below the EDS detection limit. Although the conductivity of ZnO modified BYZ is somewhat lower than the unmodified counterpart, the dramatic reduction in sintering temperature (from ~1600° to 1700°C), which will enable the exploration of a wider variety of potential electrode materials, renders the modified composition an attractive alternative to simple BYZ. Overall, the high total ionic conductivity, the high ionic transport number (>0.90 under fuel cell conditions) and good chemical stability, render BYZ-Zn4 a good candidate as an electrolyte in sensors and fuel cells.

Acknowledgments

The authors gratefully acknowledge Dr. Ma Chi for his assistance with electron microscopy and chemical analysis.

References

[1]H. Iwahara, H. Uchida, and J. Kondo, "Galvanic Cell-Type Humidity Sensor Using High-Temperature Type Proton Conductive Solid Electrolyte," *J. Appl. Electrochem.*, **13**, 265 (1983).

[2]H. Iwahara, H. Uchida, and K. Morimoto, "High-Temperature Solid Electrolyte Fuel-Cells Using Perovskite-Type Oxide Based on $BaCeO_3$," *J. Appl. Electrochem.*, **137**, 462 (1990).

[3]N. Bonanos, B. Ellis, and M. N. Mahmood, "Construction and Operation of Fuel Cells Based on the Solid Electrolyte $BaCeO_3$:Gd," *Solid State Ionics*, **44**, 305 (1991).

[4]T. Hibino, A. Hashimoto, K. Mori, and M. Sano, "A Mixed-Potential Gas Sensor Using a $SrCe_{0.95}Yb_{0.05}O_3$—Electrolyte with a Platinum Electrode for Detection of Hydrocarbons," *Electrochem. Solid-State Lett.*, **4**, H9 (2001).

[5]T. Hibino, A. Hashimoto, M. Suzuki, and M. Sano, "A Solid Oxide Fuel Cell Using Y-Doped $BaCeO_3$ with Pd-Loaded FeO Anode and $Ba_{0.5}Pr_{0.5}CoO_3$ Cathode at Low Temperatures," *J. Electrochem. Soc.*, **149**, A1503 (2002).

[6]H. Iwahara, H. Uchida, K. Ono, and K. Ogaki, "Proton Conduction in Sintered Oxides Based on $BaCeO_3$," *J. Electrochem. Soc.*, **135**, 529 (1988).

[7]R. C. T. Slade and N. Singh, "Generation of Charge-Carriers and an H/D Isotope Effect in Proton-Conducting Doped Barium Cerate Ceramics," *J. Mater. Chem.*, **1** [3] 441 (1991).

[8]W. Münch, D. Stifert, K. D. Kreuer, and J. Maier, "Quantum Molecular Dynamics Study of the Cubic Phase of $BaTiO_3$ and $BaZrO_3$," *Solid State Ionics*, **97**, 39 (1997).

[9]H. Iwahara, T. Esaka, H. Uchida, and N. Maeda, "Proton Conduction in Sintered Oxides and its Application to Steam Electrolysis for Hydrogen Production," *Solid State Ionics*, **3–4**, 359 (1981).

[10]K. C. Liang, D. Yang, and A. S. Nowick, "Fast High-Temperature Proton Transport in Nonstoichiometric Mixed Perovskites," *Solid State Ionics*, **69**, 117 (1994).

[11]B. Gross, St. Marion, R. Hempelmann, D. Grambole, and F. Hermann, "Proton Conducting $Ba_3Ca_{1.18}Nb_{1.82}O_{8.73}/H_2O$: Sol–Gel Preparation and Pressure/Composition Isotherms," *Solid State Ionics*, **109**, 13 (1998).

[12]Y. Du and A. S. Nowick, "Structural Transitions and Proton Conduction in Nonstoichiometric A(3)B′B″O-9 Perovskite-Type Oxides," *J. Am. Ceram. Soc.*, **78**, 3033 (1995).

[13]K. H. Ryu and S. M. Haile, "Chemical Stability and Proton Conductivity of Doped $BaCeO_3$–$BaZrO_3$ Solid Solutions," *Solid State Ionics*, **125**, 355 (1999).

[14]K. D. Kreuer, "On the Development of Proton Conducting Materials for Technological Applications," *Solid State Ionics*, **97**, 1 (1997).

[15]H. Iwahara, T. Yajima, T. Hibino, K. Ozaki, and H. Suzuki, "Protonic Conduction in Calcium, Strontium and Barium Zirconates," *Solid State Ionics*, **61**, 65 (1993).

[16]T. Yajima, H. Suzuki, T. Yogo, and H. Iwahara, "Protonic Conduction in $SrZrO_3$-Based Oxides," *Solid State Ionics*, **51**, 101 (1992).

[17]R. C. T. Slade, S. D. Flint, and N. Singh, "Investigation of Protonic Conduction in Yb- and Y-Doped Barium Zirconates," *Solid State Ionics*, **82**, 135 (1995).

[18]K. D. Kreuer, "Aspects of the Formation and Mobility of Protonic Charge Carriers and the Stability of Perovskite-Type Oxides," *Solid State Ionics*, **125**, 285 (1999).

[19]T. Schober and H. G. Bohn, "Water Vapor Solubility and Electrochemical Characterization of the High Temperature Proton Conductor $BaZr_{0.9}Y_{0.1}O_{2.95}$," *Solid State Ionics*, **127**, 351 (2000).

[20]H. G. Bohn and T. Schober, "Electrical Conductivity of the High-Temperature Proton Conductor $BaZr_{0.9}Y_{0.1}O_{2.95}$," *J. Am. Ceram. Soc.*, **83**, 768 (2000).

[21]A. Sin, B. El Montaser, and P. Odier, "Synthesis and Sintering of Large Batches of Barium Zirconate Nanopowders," *J. Am. Ceram. Soc.*, **85** [8] 1923 (2002).

[22]G. Tagliere, M. Tersigni, P. L. Villa, and C. Mondelli, "Synthesis by the Citrate Route and Characterisation of $BaZrO_3$, A High Tech Ceramic Oxide: Preliminary Results," *Inter. J. Inorg. Mater.*, **1**, 103 (1999).

[23]A. Azad, S. Subramaniam, and T. W. Dung, "On the Development of High Density Barium Metazirconate ($BaZrO_3$)," *J. Alloys Compounds*, **334**, 118 (2002).

[24]L. A. Chick, L. R. Pederson, G. D. Maupin, J. L. Bates, L. E. Thomas, and G. J. Exarhos, "Glycine-Nitrate Combustion Synthesis of Oxide Ceramic Powders," *Mater. Lett.*, **10**, 6 (1990).

[25]J.-L. Pouchou and F. Pichoir, pp. 31–75 in *Quantitative Analysis of Homogeneous or Stratified Microvolumes Applying the Model "PAP" in Electro Probe Quantitation*, Edited by K. Heinrich, and D. Newbut. Plenum Press, New York, 1991.

[26]J. R. MacDonald and W. B. Johnson, pp. 1–26 in *Impedance Spectroscopy*, Edited by J. R. MacDonald. Wiley and Sons, New York, 1988.

[27]A. J. Bard and L. R. Faulkner, *Electrochemical Methods*; pp. 44–54. Wiley and Sons, New York, 2001.

[28]HSC Chemistry program (Version 5.1), Outokumpu Research OY, Finland.

[29]A. C. Caballero, J. F. Fernandez, C. Moure, P. Duran, and Y. M. Chiang, "Grain Growth Control and Dopant Distribution in ZnO-Doped $BaTiO_3$," *J. Am. Ceram. Soc.*, **81** [4] 939 (1998).

[30]Y. M. Chiang, D. P. Birnie, and W. D. Kingery, *Physical Ceramics: Principles of Ceramic Science and Engineering*; pp. 376. John Wiley and Sons, New York, 1997.

[31]S. M. Haile, D. L. West, and J. Campbell, "The Role of Microstructure and Processing on the Proton Conducting Properties of Gadolinium-Doped Barium Cerate," *J. Mater. Res.*, **13**, 1576 (1998).

[32]S. M. Haile, G. Staneff, and K. H. Ryu, "Non-Stoichiometry, Grain Boundary Transport and Chemical Stability of Proton Conducting Perovskites," *J. Mater. Sci.*, **36**, 1149 (2001).

[33]T. Uda, P. Babilo, and S. M. Haile. "Thermodynamic Analysis and Conductivity of Yttrium Doped Barium Zirconate"; Ninth International Symposium on Solid Oxide Fuel Cells, The Electrochemical Society 207th Meeting, Quebec City, Canada, 2005.

[34]T. Takahashi, K. Ito, and H. Iwahara, "Efficiency of Solid-Electrolyte Fuel Cells," *Electrochim. Acta*, **12**, 21 (1967). □